Dual-Comb Spectroscopy for Rapid Characterization of Complex Optical Properties of Solids

AKIFUMI ASAHARA,[1,2] AKIKO NISHIYAMA,[1,2] SATORU YOSHIDA,[1,2] KEN-ICHI KONDO,[1,2] YOSHIAKI NAKAJIMA[1,2] AND KAORU MINOSHIMA[1,2,*]

[1]Department of Engineering Science, Graduate School of Informatics and Engineering, The University of Electro-Communications (UEC), 1-5-1 Chofugaoka, Chofu, Tokyo 182-8585 Japan
[2]JST, ERATO, MINOSHIMA Intelligent Optical Synthesizer (IOS) Project, 1-5-1 Chofugaoka, Chofu, Tokyo 182-8585 Japan
*Corresponding author: k.minoshima@uec.ac.jp

We demonstrate rapid characterization of complex optical properties of solids via dual-comb spectroscopy (DCS) in the near-infrared region. The fine spectral structures in the complex refractive index of an Er:YAG are successfully deduced using the developed system and Fourier analysis. Moreover, simultaneous determination of the refractive index and the thickness is demonstrated for a silicon semiconductor wafer through the use of multi-reflected echo signals. The results indicate the potential of DCS as a powerful measurement tool for the rapid and full-characterization of solid materials.

Continued development of fast and superior techniques characterizing the optical properties of materials, such as refractive index and absorption, with precise spectral information is essential. In general, the amplitude of the reflectance and transmittance has been commonly employed to investigate materials. When complex properties with phase information are required, they can be deduced using the Kramers-Kronig relations. However, in principle, since the relations need wide spectral information to elicit an accurate spectrum, direct observation of the phase is preferable. There are several methods to directly observe phase information, such as ellipsometry, interferometric Fourier measurement, and spatially dispersive comb spectroscopy [1].

Dual-comb spectroscopy (DCS) is an attractive direct comb spectroscopy using dual, slightly asynchronized optical-frequency-combs [2, 3]. DCS is a phase-sensitive interferometric method; the first comb (the signal comb) stores the information of the sample properties, and the second comb (the local comb) retrieves it as an interference signal in the time-domain, enabling direct detection of both the real and imaginary parts of the optical properties without making complicated assumptions. DCS has many advantages compared to conventional Fourier transform spectroscopy. By taking advantage of the accurate and coherent pulse controllability of the frequency comb, precise spectral detection with high frequency resolution can be achieved over a wide frequency range, and a high signal-to-noise ratio (SNR) and rapid data acquisition can also be achieved inherently.

DCS has progressed mainly in the field of high-precision spectroscopy in the near-infrared region for molecular gas [3], as its ultra-high frequency resolution and its ultra-high accuracy of absolute frequency have attracted significant attention. Meanwhile, efforts have been made in the development of efficient data acquisition schemes, such as coherent averaging [3] and adaptive sampling [4, 5]. Recently, the available frequency range for DCS has widened from terahertz to ultraviolet with current frequency conversion techniques [6-9]. Moreover, the application of DCS has been cleverly extended to the observation of other interesting phenomena, for instance, nonlinear coherent Raman spectroscopy [10] and two-photon excitation spectroscopy [11]. Here, as a new application, we propose the use of DCS for characterization of solids, such as semiconductors, oxides, and laser media. In some previous works, the complex transmittance of metamaterials [12] and of fiber components [13], the transmittance of microresonators [14], and the absorption of Nd ion [15] have been observed. However, to our knowledge, more detailed characterization of solids has not been focused on despite their importance in the field.

In this letter, we demonstrate the characterization of complex optical properties of solids via DCS in the near-infrared region. Fine spectral structures in the complex refractive index of an Er:YAG (Yttrium Aluminum Garnet: $Y_3Al_5O_{12}$) are successfully deduced using the developed system and a Fourier model analysis. Moreover, simultaneous determination of both the refractive index and the thickness is demonstrated for a silicon semiconductor wafer through the use of multi-reflected echo signals. DCS enables the rapid monitoring of the complex optical properties of solids.

A schematic of the developed DCS system is shown in Fig. 1. We employed two lab-built Er-doped fiber combs, mode-locked via nonlinear polarization rotation. The center frequencies and full-width half maximum bandwidths of the combs were ~192 THz (~1560 nm) and ~5 THz (~41 nm), respectively. The pulse durations were a few picoseconds, broadened because of chirp in the fiber. In the following experiments, the repetition rates of the signal and local combs, $f_{rep,S}$ and $f_{rep,L}$, were ~56 MHz, and the frequency difference, $\Delta f_{rep} = f_{rep,S} - f_{rep,\,L}$, was set to ~120.6 Hz, so that the carrier frequency bandwidth was included in the ~13.3-THz Nyquist optical bandwidth, $f_{rep,S} \cdot f_{rep,L}/2\Delta f_{rep}$.
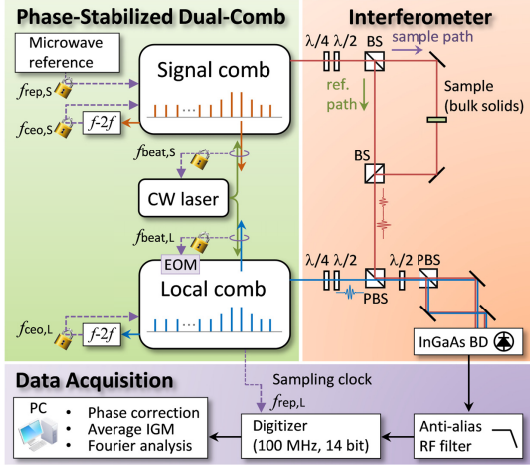
Fig. 1. Schematic of the developed dual-comb spectroscopic system; f–$2f$: an f–$2f$ self-reference interferometer; EOM: electro-optic modulator; BD: balanced detector; IGM: interferogram.

Tight and coherent phase stabilization between the two combs was achieved using electronic feed-back control with a ~1560-nm slave continuous-wave laser (PLANEX, Redfern Integrated Optics). In the signal comb, the offset frequency $f_{ceo,S}$, monitored by the f–$2f$ self-referencing method, was stabilized using the pump current injection control, and $f_{rep,S}$ was stabilized using the piezoelectric and temperature control. The frequencies of the optical modes were phase-stabilized to the microwave clock with reference to a global positioning system (FT-001, Freqtime, 3.2×10^{-12} at 1 s). The slave laser was locked by stabilizing the beat signal with one mode of the signal comb, $f_{beat,S}$. In the local comb, $f_{ceo,L}$ was stabilized using a similar pump current injection control, while $f_{rep,L}$ was locked by stabilizing the beat signal with the slave laser, $f_{beat,L}$. Here, the error signal was fed back to the piezo, the temperature, and the intra-cavity electro-optic modulator inserted in the local comb, enabling fast servo control [16]. As a result, the relative linewidth achieved between the two combs was a few mHz, corresponding to a coherence time far longer than 1 s, which is sufficient for coherent integration of the interference signal.

The output from the signal comb was divided into sample and reference paths. Each transmitted pulse, with some time interval, was spatially combined with the local comb. The interference signal (IGM: interferogram) was detected using a balance detection system with an InGaAs fast detector (80-MHz bandwidth, 1817-FS, Newport). The IGM was passed through anti-alias filters (~30-MHz low-pass filters), and was sampled by a digitizer (100-MHz

bandwidth, 14-bit resolution, PXIe-5122, National Instruments) synchronized to the repetition rate of the local comb, $f_{rep,L}$.

As a demonstration, we characterized an Er:YAG ceramic (50% doped, ~550 μm thick) and a high-resistivity Si semiconductor wafer (~730 μm thick). All the experiments were performed at room temperature in ambient pressure.
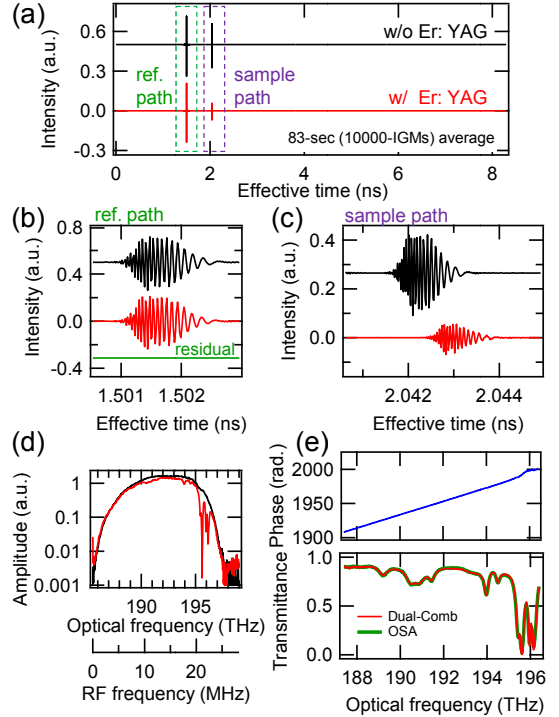
Fig. 2. (a) Interferograms (IGM) observed for Er:YAG, with (w/) and without (w/o) the sample. "Effective time" denotes the time interval between sweeping pulses of the signal and local combs. (b) The expanded IGMs for the reference path and the residual between the IGMs with and without the sample. (c) The expanded IGMs for the sample path. (d) Fourier-transformed amplitude spectra for the IGMs for the sample path with (red) and without (black) the sample. (e) The complex transmittance spectra of the Er:YAG, phase (upper) and magnitude (lower), compared with the transmittance spectrum observed by an optical spectrum analyzer (OSA).

First, Fig. 2(a) shows the IGMs observed for the Er:YAG, with and without the sample. The left and right spike-shaped signals represent the center-bursts corresponding to the signal comb passed through the reference and sample paths, respectively.

The expanded "reference IGMs" are shown in Fig. 2(b). For persistent coherent averaging, we applied a computational real-time phase compensation scheme, called the Forman method [9, 17]. As a result, the phase relative to the IGM's envelope was kept constant during each measurement as found from the residual data in Fig. 2(b), and a long coherent data integration time far longer than the relative coherence time (>1 s) was achieved.

In Fig. 2(c), the expanded "sample IGMs" are displayed. Here, the relative coherence between the two IGMs was assured by the phase compensation. By inserting the Er:YAG into the system, a several-picosecond delay was observed in the IGMs because of the change of the optical path length. Meanwhile, the amplitude of the IGM decreased as a result of the reflection and absorption. From

both the observed amplitude and phase information, the complex properties of the sample can be deduced as follows.

First, the Fourier-transformed amplitude spectra, corresponding to the multiplication of the amplitude spectra of the signal and local combs, were obtained as shown in Fig. 2(d). In the transformation process, a part of the IGM around only the center burst was cut out, resulting in a ~27-GHz frequency resolution. Higher frequency resolution can be obtained by tailoring the process if necessary. This moderate resolution is sufficient to resolve the broadened spectra typically found in the range of the experimental conditions in this study, and has the benefit of reducing the real-time calculation cost. Some zeros were padded to the extracted waveforms to obtain smooth spectra. In the spectrum, the fine absorption structure due to the doped Er^{3+} ions is clearly identical. The SNR of the spectrum is evaluated to be the order of 10^3 after ~83 s of data acquisition (corresponding to 10,000 IGMs), and is linearly improved to the square root of the acquisition time.

Next, the complex transmittance spectrum $\tilde{T}(\omega)$ of the sample was calculated. In fact, if we simply normalize the Fourier-transformed spectra as $\tilde{T}(\omega) = \mathcal{F}\big[\text{IGM}^{\text{sam}}_{\text{w/}}(t)\big]/\mathcal{F}\big[\text{IGM}^{\text{sam}}_{\text{w/o}}(t)\big]$, a slow spectral distortion due to the fluctuation of the system is imposed. Here, the super- and the sub-scripts denote the corresponding path and the existence of the sample, as defined in Figs. 2(a)-2(c). In order to avoid deterioration of the data, we applied the following scheme: First, without the sample in advance, we assessed the ratio of the optical transfer functions of the sample and reference paths as $\tilde{R}(\omega) \equiv \mathcal{F}\big[\text{IGM}^{\text{sam}}_{\text{w/o}}(t)\big]/\mathcal{F}\big[\text{IGM}^{\text{ref}}_{\text{w/o}}(t)\big]$. Subsequently, with the sample, $\tilde{T}(\omega)$ was calculated for each periodic IGM observed within every $1/\Delta f_{\text{rep}}$ as $\tilde{T}(\omega) = \mathcal{F}\big[\text{IGM}^{\text{sam}}_{\text{w/}}(t)\big]/\big\{\tilde{R}(\omega) \cdot \mathcal{F}\big[\text{IGM}^{\text{ref}}_{\text{w/}}(t)\big]\big\}$, and was integrated for the total acquisition time. In this way, the slow spectral fluctuation of the comb sources can be canceled out and an accurate characterization of $\tilde{T}(\omega)$ can be achieved. Here, the fluctuation of $\tilde{R}(\omega)$ was small enough to be neglected.

Figure 2(e) shows the complex transmittance spectrum $\tilde{T}(\omega)$ observed using this scheme. In the amplitude spectrum, the fine absorption lines attributed to the Stark levels of the Er^{3+} ion ($^4I_{15/2} \rightarrow {}^4I_{13/2}$) were clearly resolved. The spectral structure corresponded well to that obtained by a white lamp and an optical spectrum analyzer with a resolution of ~60 GHz (0.5 nm). The unwrapped phase spectrum was roughly linear versus the frequency, and had small bumpy structures around 196 THz where the large absorption peaks were located.

In general, when the complex transmittance $\tilde{T}(\omega)$ of a sample is given, its complex optical properties (refractive index $\tilde{n}(\omega)$, permittivity $\tilde{\varepsilon}(\omega)$, conductivity $\tilde{\sigma}(\omega)$, etc.) can be deduced through a self-consistent analysis with an appropriate model. In this study, we applied a simple transmission model, where probe light propagates through a uniform dielectric slab. When the multi-reflected signals are neglected, $\tilde{T}(\omega)$ can be given as:

$$\tilde{T}(\omega) = \frac{4\tilde{n}n_{\text{air}}}{(\tilde{n}+n_{\text{air}})^2}\exp\left(i\frac{(\tilde{n}-n_{\text{air}})d}{c}\omega\right), \quad (1)$$

where n_{air} is the refractive index of the ambient air (≈ 1.00026), d is the thickness of a sample, and c is the speed of light in a vacuum.

With this model, the complex refractive-index spectrum of the Er:YAG was deduced using the successive approximation method, which has often been used in terahertz time-domain spectroscopy

[18], and the result is shown in Fig. 3. Here, we note that the complex optical properties could be directly obtained in the near-infrared region without performing the Kramers–Kronig transformation. The real part (refractive index $n(\omega)$) closely resembled the differential of the imaginary part (extinction coefficient $\kappa(\omega)$) as expected from the relations, which is clearly shown in the inset of Fig. 3. The value of the index, $n \approx 1.83$, was consistent with the literature [19]; the refractive index of non-doped YAG is estimated to be ~1.81 at 1.56 µm and the deviation can be attributed to a slight change in the index due to the dopant. In the current experiment, the uncertainty in the estimated index was mainly due to the uncertainty in the thickness (±10 µm) measured with a Vernier caliper, which could also have contributed to the difference of the n value. With the addition of a scheme for precise thickness evaluation, the accuracy of index characterization will be further improved; an example will be shown later.
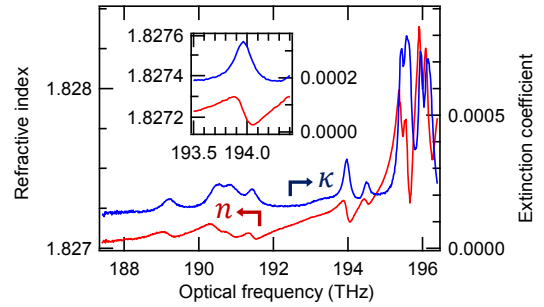
Fig. 3. Deduced complex refractive-index spectrum of the Er:YAG ceramic (red: refractive index n, blue: extinction coefficient κ). The inset shows the magnification of the plot around 194 THz.

In this way, the complex optical properties of an Er:YAG can be characterized with the developed DCS system and the Fourier analysis. The fine spectral structures of both the real and imaginary parts of the refractive index can be observed directly and rapidly. As for the frequency resolution, adjusted to GHz in this experiment, we note that it can be optimized according to the application. The duty cycle of the available data, ~1/482 in this case, will be improved by adopting sources with higher repetition rates in the gigahertz range, such as electrically modulated comb generators [20] or mode-filtered combs with a Fabry–Pérot cavity.

Next, we demonstrate, for transparent materials with high refractive index, the index and thickness of the sample can be determined simultaneously through the use of the multi-reflected echo signals, using the following scheme. As a demonstration, we characterized a silicon semiconductor wafer.

Figure 4(a) shows the observed IGMs corresponding to the sample path, with and without the Si wafer. The same experimental conditions as for the Er:YAG were applied. With the sample, the multi-reflected echo signal was clearly observed after a fundamental burst, because silicon has a high refractive index (larger than 3) in this frequency region.

This data was analyzed as follows. First, we cut out the data around the fundamental burst and the first echo, defining $\text{IGM}^{\text{sam}}_{\text{fund}}(t)$ and $\text{IGM}^{\text{sam}}_{\text{echo}}(t)$, respectively. Then, the effective complex transmittances were calculated as $\tilde{T}_{\text{fund}}(\omega) = \mathcal{F}[\text{IGM}^{\text{sam}}_{\text{fund}}(t)]/\mathcal{F}\big[\text{IGM}^{\text{sam}}_{\text{w/o}}(t)\big]$ and $\tilde{T}_{\text{echo}}(\omega) = \mathcal{F}[\text{IGM}^{\text{sam}}_{\text{echo}}(t)]/$

$\mathcal{F}\left[\text{IGM}_{\text{w/o}}^{\text{sam}}(t)\right]$. Figure 4(b) shows the calculated phase spectra, ϕ_{fund} and ϕ_{echo}, which exhibit almost linear spectra versus the frequency. When the sample is transparent to the probe light, the phase shift at the surface can be neglected, and the slope of the phase spectrum of the transmittance corresponds to the optical path length. Hence, the phase spectra can be expressed as:

$$\phi_{\text{fund}}(\omega) = \frac{\omega d}{c}(n - n_{\text{air}}), \qquad (2)$$

$$\phi_{\text{echo}}(\omega) = \frac{\omega d}{c}(3n - n_{\text{air}}). \qquad (3)$$
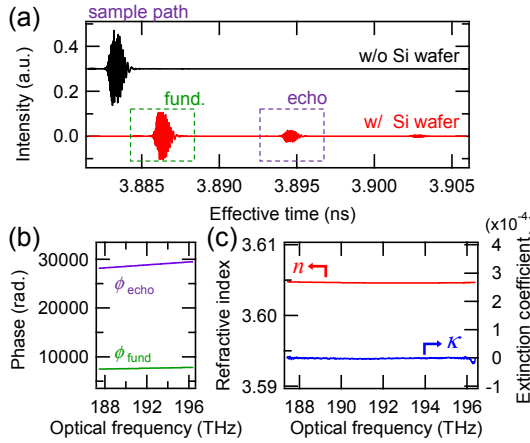
Fig. 4. (a) IGMs observed for the Si wafer, with (red) and without (black) the sample. (b) Phase spectra of ϕ_{fund} and ϕ_{echo}. (c) Deduced complex refractive-index spectrum of the Si wafer.

From these relations, the average refractive index in the frequency range of interest, n_{ave}, and the thickness d can be simultaneously evaluated by fitting the slopes. As a result, n_{ave} and d were evaluated as 3.605 and 730.4 µm, respectively. The obtained index was consistent with typically observed value in silicon, for example with a data observed from spectral interferometry [21]. Furthermore, the spectrum can be determined with $\tilde{T}_{\text{fund}}(\omega)$ and the evaluated thickness d using the successive approximation method. The resulting complex refractive index $\tilde{n}(\omega)$ is shown in Fig. 4(c). The refractive index $n(\omega)$ was deduced near n_{ave} and the extinction coefficient $\kappa(\omega)$ was almost zero as expected. In this way, the refractive index in the near-infrared region and the thickness of the Si wafer can be characterized simultaneously using the DCS system.

In conclusion, we demonstrated DCS for the characterization of solids. Rapid characterization of the complex optical properties of an Er:YAG was successfully achieved using the developed DCS system. The fine real and imaginary parts of the refractive-index spectra due to the Er^{3+} dopant were clearly obtained with a GHz resolution in the near-infrared region without performing the Kramers-Kronig transformation. Simultaneous characterization of the refractive index and thickness of a silicon semiconductor wafer was also demonstrated using multi-reflected echo signals.

Such DCS measurement with moderate (but sufficiently high for solids) resolution is useful for rapid characterization of solids, and will exhibit its unique potential especially for solids showing fine spectral components, such as excitons observed in semiconductors at low temperatures.

The schemes demonstrated here have great potential for being extended. For example, the applicable frequency regions can be extended through the use of current frequency conversion techniques [6-9]. A reflection configuration can be applied for opaque materials. Materials with other configurations, such as thin films or mixed materials, can be applied using the corresponding models [18], such as Thinkam's theory or effective medium theory. The rapid acquisition can enable even real-time monitoring of complex properties of solids. Polarization measurements can investigate a complex dielectric tensor, accessing birefringence, Verdet constant, *etc.* Moreover, by combining with a pump-probe method, coherent time-resolved comb spectroscopy will be realized. In this way, DCS has great potential as a powerful tool for rapid and complete characterization in a range of applications.

References

1. S. K. Scholten, J. D. Anstie, N. B. Hébert, R. T. White, J. Genest, and A. N. Luiten, Opt. Lett. **41**, 1277 (2016).
2. F. Keilmann, C. Gohle, and R. Holzwarth, Opt. Lett. **29**, 1542 (2004).
3. I. Coddington, N. Newbury, and W. Swann, Optica **3**, 414 (2016).
4. T. Ideguchi, A. Poisson, G. Guelachvili, N. Picqué, and T. W. Hänsch, Nat. Commun. **5**, 3375 (2014).
5. J. Roy, J.-D. Deschênes, S. Potvin, and J. Genest, Opt. Express **20**, 21932 (2012).
6. E. Baumann, F. R. Giorgetta, W. C. Swann, A. M. Zolot, I. Coddington, and N. R. Newbury, Phys. Rev. A **84**, 062513 (2011).
7. T. Ideguchi, A. Poisson, G. Guelachvili, T. W. Hänsch, and N. Picqué, Opt. Lett. **37**, 4847 (2012).
8. Y. Jin, S. M. Cristescu, F. J. M. Harren, and J. Mandon, Appl. Phys. B **119**, 65 (2015).
9. S. Okubo, K. Iwakuni, H. Inaba, K. Hosaka, A. Onae, H. Sasada, and F.-L. Hong, Appl. Phys. Exp. **8**, 082402 (2015).
10. T. Ideguchi, S. Holzner, B. Bernhardt, G. Guelachvili, N. Picqué, and T. W. Hänsch, Nature **502**, 355 (2013).
11. A. Hipke, S. A. Meek, T. Ideguchi, T. W. Hänsch, and N. Picqué, Phys. Rev. A **90**, 011805(R) (2014).
12. T. Ganz, M. Brehm, H. G. von Ribbeck, D. W. van der Weide, and F. Keilmann, New J. Phys. **10**, 123007 (2008).
13. P. M.-Mateos, M. R.-Llata, J. P.-Roman, and P. Acedo, IEEE Photon. Technol. Lett. **27**, 1309 (2015).
14. V. M.-Belleau, J. Roy, S. Potvin, J.-R. Carrier, L.-S. Verret, M. Charlebois, J. Genest, and C. N.-Allen, Opt. Express **20**, 3066 (2012).
15. T. Ideguchi, T. Nakamura, Y. Kobayashi, and K. Goda, Optica **3**, 748 (2016).
16. Y. Nakajima, H. Inaba, K. Hosaka, K. Minoshima, A. Onae, M. Yasuda, T. Kohno, S. Kawato, T. Kobayashi, T. Katsuyama, and F.-L. Hong, Opt. Express **18**, 1667 (2010).
17. M. L. Forman, W. H. Steel, and G. A. Vanasse, J. Opt. Soc. Am. **56**, 59 (1966).
18. J. L.-Hughes and T.-I. Jeon, J. Infrared Millim. Te. **33**, 871 (2012).
19. A. A. Kaminskii, K. Ueda, A. F. Konstantinova, H. Yagi, T. Yanagitani, A. V. Butashin, V. P. Orekhova, J. Lu, K. Takaichi, T. Uematsu, M. Musha, and A. Shirokava, Crystallogr. Rep. **48**, 868 (2003).
20. M. Kourogi, K. Nakagawa, and M.Ohtsu, IEEE J. Quantum Elect. **29**, 2693 (1993).
21. J. Park, J. Jin, J. W. Kim, and J.-A. Kim, Opt. Commun. **305**, 170 (2013).

Full References

1. S. K. Scholten, J. D. Anstie, N. B. Hébert, R. T. White, J. Genest, and A. N. Luiten, "Complex direct comb spectroscopy with a virtually imaged phased array," Opt. Lett. **41**(6), 1277-1280 (2016).

2. F. Keilmann, C. Gohle, and R. Holzwarth, "Time-domain mid-infrared frequency-comb spectrometer," Opt. Lett. **29(**13), 1542-1544 (2004).

3. I. Coddington, N. Newbury, and W. Swann, "Dual-comb spectroscopy," Optica **3**(4), 414-426 (2016).

4. T. Ideguchi, A. Poisson, G. Guelachvili, N. Picqué, and T. W. Hänsch, "Adaptive real-time dual-comb spectroscopy," Nat. Commun. **5**, 3375 (2014).

5. J. Roy, J.-D. Deschênes, S. Potvin, and J. Genest, "Continuous real-time correction and averaging for frequency comb interferometry," Opt. Express **20**(20), 21932-21939 (2012).

6. E. Baumann, F. R. Giorgetta, W. C. Swann, A. M. Zolot, I. Coddington, and N. R. Newbury, "Spectroscopy of the methane $_3$ band with an accurate midinfrared coherent dual-comb spectrometer," Phys. Rev. A **84**, 062513 (2011).

7. T. Ideguchi, A. Poisson, G. Guelachvili, T. W. Hänsch, and N. Picqué, "Adaptive dual-comb spectroscopy in the green region," Opt. Lett. **37**(23), 4847-4849 (2012).

8. Y. Jin, S. M. Cristescu, F. J. M. Harren, and J. Mandon, "Femtosecond optical parametric oscillators toward real-time dual-comb spectroscopy," Appl. Phys. B **119**, 65-74 (2015).

9. S. Okubo, K. Iwakuni, H. Inaba, K. Hosaka, A. Onae, H. Sasada, and F.-L. Hong, "Ultra-broadband dual-comb spectroscopy across 1.0–1.9 μm," Appl. Phys. Exp. **8**, 082402 (2015).

10. T. Ideguchi, S. Holzner, B. Bernhardt, G. Guelachvili, N. Picqué, and T. W. Hänsch, "Coherent Raman spectro-imaging with laser frequency comb," Nature **502**, 355-359 (2013).

11. A. Hipke, S. A. Meek, T. Ideguchi, T. W. Hänsch, and N. Picqué, "Broadband Doppler-limited two-photon and stepwise excitation spectroscopy with laser frequency combs," Phys. Rev. A **90**, 011805(R) (2014).

12. T. Ganz, M. Brehm, H. G. von Ribbeck, D. W. van der Weide, and F. Keilmann, "Vector frequency-comb Fourier-transform spectroscopy for characterizing metamaterials," New J. Phys. **10**, 123007 (2008).

13. P. M.-Mateos, M. R.-Llata, J. P.-Roman, and P. Acedo, "Dual-comb architecture for fast spectroscopic measurements and spectral characterization," IEEE Photon. Technol. Lett. **27**(12), 1309-1312 (2015).

14. V. M.-Belleau, J. Roy, S. Potvin, J.-R. Carrier, L.-S. Verret, M. Charlebois, J. Genest, and C. N.-Allen, "Whispering gallery mode sensing with a dual frequency comb probe," Opt. Express **20**(3), 3066-3075 (2012).

15. T. Ideguchi, T. Nakamura, Y. Kobayashi, and K. Goda, "Kerr-lens mode-locked bidirectional dual-comb ring laser for broadband dual-comb spectroscopy," Optica **3**(7), 748-753 (2016).

16. Y. Nakajima, H. Inaba, K. Hosaka, K. Minoshima, A. Onae, M. Yasuda, T. Kohno, S. Kawato, T. Kobayashi, T. Katsuyama, and F.-L. Hong, "A multi-branch, fiber-based frequency comb with millihertz-level relative linewidths using an intra-cavity electro-optic modulator," Opt. Express **18**(2), 1667-1676 (2010).

17. M. L. Forman, W. H. Steel, and G. A. Vanasse, "Correction of asymmetric interferograms obtained in Fourier spectroscopy," J. Opt. Soc. Am. **56**(1), 59-63 (1966).

18. J. L.-Hughes and T.-I. Jeon, "A review of the terahertz conductivity of bulk and nano-materials," J. Infrared Millim. Te. **33**, 871 (2012).

19. A. A. Kaminskii, K. Ueda, A. F. Konstantinova, H. Yagi, T. Yanagitani, A. V. Butashin, V. P. Orekhova, J. Lu, K. Takaichi, T. Uematsu, M. Musha, and A. Shirokava, "Refractive indices of laser nanocrystalline ceramics based on $Y_3Al_5O_{12}$," Crystallogr. Rep. **48**(5), 868-871 (2003).

20. M. Kourogi, K. Nakagawa, and M.Ohtsu, "Wide span optical frequency comb generator for accurate optical frequency difference measurement," IEEE J. Quantum Elect. **29**(10), 2693-2701 (1993).

21. J. Park, J. Jin, J. W. Kim, and J.-A. Kim, "Measurement of thickness profile and refractive index variation of a silicon wafer using the optical comb of a femtosecond pulse laser," Opt. Commun. **305**, 170-174 (2013).